Experimental band structure of potassium as measured by angle-resolved photoemission

B. S. Itchkawitz, In-Whan Lyo,* and E. W. Plummer
Department of Physics, University of Pennsylvania, Philadelphia, Pennsylvania 19104-6396
(Received 27 July 1989)

The bulk band structure of potassium along the [110] direction was measured using angle-resolved photoemission from an epitaxial potassium film several thousand angstroms thick grown on a Ni(100) substrate. We find the occupied bandwidth to be 1.60 ± 0.05 eV, which is narrower than the free-electron bandwidth of 2.12 eV and agrees with recent calculations of the quasiparticle self-energy. A narrow peak near the Fermi level which did not disperse with photon energy was observed for photon energies which, according to the nearly-free-electron model, should yield no direct transitions. A comparison of the binding energy and intensity of the anomalous peak as functions of photon energy is made to the calculations of Shung and Mahan [Phys. Rev. B **38**, 3856 (1988)]. The discrepancies found are discussed in terms of an enhanced surface photoeffect in the photon energy range $20 \leq \hbar\omega \leq 30$ eV. For low photon energies, a bulk peak was also observed due to a surface umklapp process with an intensity comparable to the standard bulk (110) peak. The possible contributions to this strong surface umklapp process from a shear instability at the first few (110) atomic planes is discussed.

I. INTRODUCTION

Since the alkali metals bear the closest resemblance to the approximations made in one-electron theories of the electronic properties of metals, examination of their electronic structure should illuminate deficiencies in the one-electron picture. Previous angle-resolved photoemission studies of the Na(110) surface[1,2] have revealed features which cannot be explained by the independent-particle model of photoemission. These features include an occupied bandwidth 18% narrower than the nearly-free-electron (NFE) model predicts, and an anomalous sharp peak seen near the Fermi level for ranges of photon energies which should yield no direct transitions. The narrowing of the Na bandwidth occurs because one-electron excitations from the NFE ground state do not include the self-energy and therefore do not correctly model the true excitation spectra of metals. Numerous calculations[2-4] which use various approximations and computational techniques to go beyond the independent-particle model have successfully computed the occupied bandwidth narrowing of Na as measured by photoemission due to the quasiparticle self-energy. The suggested explanations of the anomalous peak near the Fermi level in Na include a surface resonance 0.75 eV above the Fermi level,[5] band distortions due to the presence of a charge-density wave (CDW),[6] and broadening of the final states due to the finite mean free path of the electrons.[4] Each model is successful in explaining some aspect of the behavior of the anomalous peak, but only the analysis of Shung and Mahan[4] (SM) of the effects of the final-state broadening is detailed enough to make more than a cursory comparison to experimental results. While SM cannot explain the existence of the anomalous peak at photon energies for which the standard bulk peak is also seen, their calculations of the binding energy and intensity of the anomalous peak as a function of photon energy for Na compare very well with experiment.

To discriminate between the various theories for the occupied bandwidth narrowing and the anomalous Fermi-level peak, we performed angle-resolved photoemission from the K(110) surface. We obtained a measured occupied bandwidth 25% smaller than that predicted by the NFE theory, which agrees well with recent many-body calculations of the self-energy.[2,4,7] We observed a sharp peak near the Fermi level as seen in Na, but the binding energy and intensity of the peak in K are qualitatively different from those in Na, suggesting problems with the final-state-broadening explanation. We also observed a dispersing peak at low photon energies which we attribute to photoelectrons undergoing an additional surface umklapp scattering process.

II. EXPERIMENTAL DETAILS

The experiment was performed at the National Synchrotron Light Source (NSLS) vuv beamline U-12 at Brookhaven National Laboratory (Upton, NY). The beamline is equipped with a toroidal-grating monochromator and an angle-resolved hemispherical electron-energy analyzer which have been described elsewhere.[8] The photons were incident on the sample at 45° from the sample normal and were polarized in the plane of incidence. The energy analyzer has an acceptance angle of $\pm2°$ and the total instrumental energy resolution was 0.2 eV at 25 eV, 0.3 eV at 45 eV, and 0.4 eV at 100 eV.

Epitaxial potassium films thousands of angstroms thick were grown by depositing potassium from a getter source onto a Ni(100) substrate cooled to ~160 K and then annealing the film to ~270 K. This procedure yielded films which exhibited faint low-energy electron-diffraction (LEED) patterns indicative of a bcc (110) structure. Photoemission spectra were taken with the sample at 95 K. The cleanliness of the film was verified by monitoring the

oxygen photoemission peak which occurs at about 3 eV below the Fermi level. The sample became contaminated with oxygen only where the photon beam was incident. We were therefore able to move the sample every few scans to continue taking data from a clean region without having to grow a new film.

III. MEASURED DISPERSION

The standard picture of photoemission assumes energy and reduced momentum conservation, as expressed by

$$E_f(\mathbf{k}\pm\mathbf{G})=E_i(\mathbf{k})+\hbar\omega\ , \tag{1}$$

where E_i and E_f are the initial and final electron energies, $\mathbf{k}$ is the electron's initial momentum in the reduced-zone scheme, $\mathbf{G}$ is a bulk reciprocal-lattice vector, and $\hbar\omega$ is the energy of the incident photon. Energy conservation requires that the final-state energy equal the initial-state energy plus the photon energy. Momentum can only be conserved in the photoemission process by including a reciprocal-lattice vector $\mathbf{G}$ in the transition. In the reduced-zone picture, momentum conservation requires that the transition from occupied states below the Fermi level to unoccupied states above E_F be vertical. Only transitions which conform to the conservation criteria will result in a peak in a photoemission energy-distribution curve (EDC). In the free-electron picture for K along the [110] or Σ direction, as shown by the solid line in Fig. 1, the only transition which can occur for 38-eV photons would produce a peak about 1.9 eV below E_F. Note that for certain ranges of photon energies, called photon-energy gaps, none of the occupied states can satisfy the conservation criteria. Within these photon-energy gaps, 20.7–24.5 and 63.3–69.7 eV, no direct transitions may occur. For example, for $\hbar\omega=69$ eV, the conservation criteria can only be satisfied by an unoccupied initial state.

Figure 2 shows a series of low-photon-energy EDC's taken at normal emission, corresponding to the Σ direction in $\mathbf{k}$ space, which illustrates some of the features seen. The intensity of Fig. 2(b) is multiplied by a factor of 5.5 with respect to Fig. 2(a) to illustrate the weak structures. The peak at about -3 eV is from a very small amount of oxygen contamination. Comparison to recent photoemission studies of oxygen on alkali metals[9] shows that our oxygen contamination is well below the equivalent of a 0.05-L exposure to O_2. [1 langmuir (L)$\equiv 10^{-6}$ Torr sec.] The photoemission cross section of K is very low for two reasons: the bands are weakly cou-

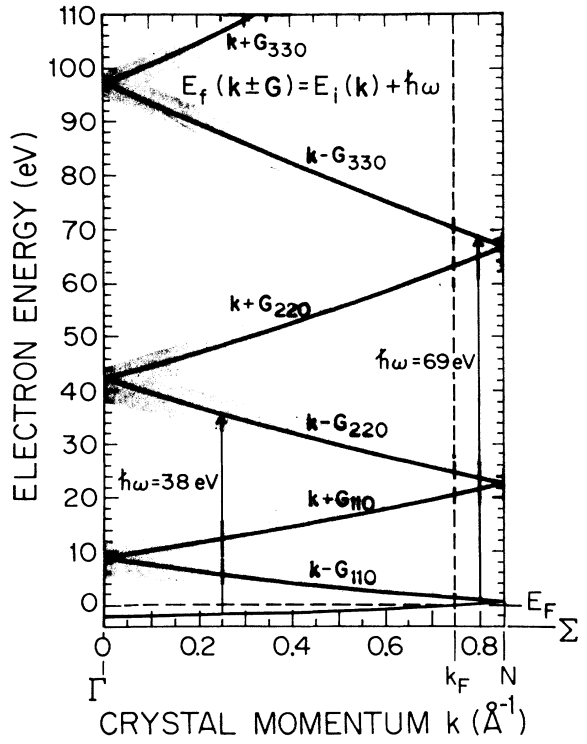

FIG. 1. Free-electron bands along the Σ axis in K. The shaded region illustrates the broadening of the final states due to the photoelectron's finite mean free path. Energy and momentum conservation require photoemission transitions to be vertical in the reduced zone. For $\hbar\omega=38$ eV the transition should produce a peak about 1.9 eV below the Fermi level in an EDC. In certain photon-energy ranges, e.g., $\hbar\omega=69$ eV, no occupied states can meet the conservation criteria, so no peak is expected.

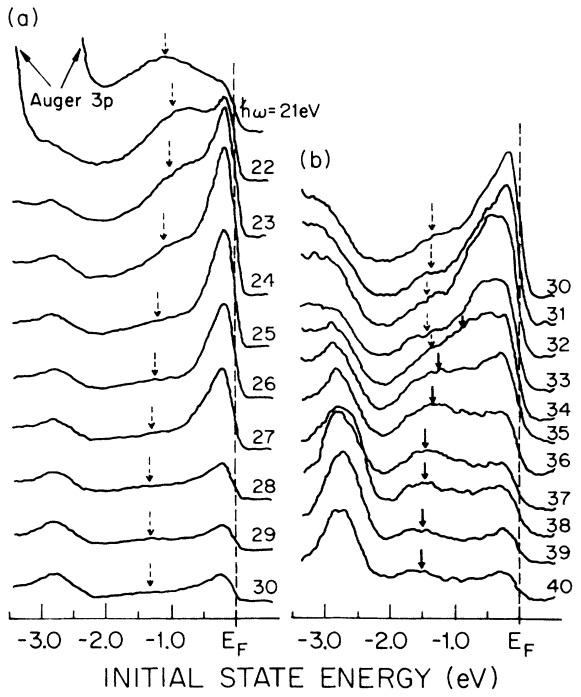

FIG. 2. Series of normal-emission EDC's from K(110) for photon energies of 21–40 eV. (b) is multiplied by a factor of 5.5 with respect to (a) to illustrate the weak structures. The most striking feature of the spectra is the large peak at the Fermi level, which is clearly seen at photon energies that should not yield direct transitions. Solid arrows signify bulk (110) peak dispersion and dashed arrows signify surface umklapp peak dispersion. The peak at ~ -3 eV is from a small amount of oxygen contamination. The intense peak seen for $\hbar\omega=21$, and 22 eV is the Auger $3p$ level of K.

pled to the lattice psuedopotential, and the occupied s bands are delocalized and have a small occupancy, as compared to the d or f bands of other metals. Because of the low cross section to photoemission, the peaks in the EDC's from K are weak and require long acquisition times of up to 45 min for reasonable signal-to-noise ratios. The Auger $3p$ level of K has a kinetic energy of 18.3 eV and, for the lower photon energies shown in Fig. 2(a), is seen to move toward higher binding energies as the photon energy is increased. The lower photon-energy gap extends from $\hbar\omega=20.7$ to 24.5 eV, yet in this range there is clearly a sharp and intense peak near the Fermi level and a weaker dispersing peak around -1.3 eV that we will attribute to a surface umklapp process (dashed arrows). For higher photon energies, shown in Fig. 2(b), the standard bulk (110) peak (solid arrows) disperses away from the Fermi level, while the peak we attribute to a surface umklapp process disperses toward the Fermi level and weakens.

Figure 3 shows the dispersion of the initial-state energy as a function of photon energy for the observed peaks. The dispersion of the binding energy of the peaks as a function of photon energy has information on both the initial- and final-state dispersions. The dashed lines describe the dispersion predicted by requiring energy and momentum conservation for transitions among the free-electron bands along the [110] direction (normal to the surface). At photon energies of 44 and 99 eV, transitions occur from the bottom of the band at the Γ point. The two photon-energy gaps at 20.7–24.5 and 63.3–69.7 eV are defined by the photon energies for which the NFE initial state crosses the Fermi level.

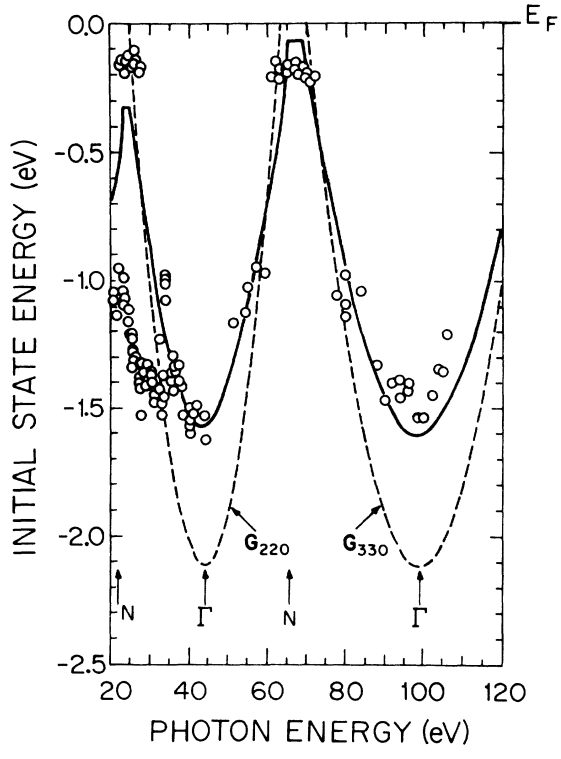

FIG. 3. Initial-state energy as a function of photon energy $\hbar\omega=20$–120 eV for K(110) normal emission. Instrumental resolution has not been removed. Circles are experimental data. Dashed line is the dispersion from the NFE model and the solid line is our calculation of the NFE dispersion with an occupied bandwidth of 1.60 eV including the effects of initial- and final-state broadening.

The lack of data points for photon energies between 45 and 50 eV and greater than 110 eV is due to the reduced efficiency of the monochromator gratings at these photon energies. When the initial-state peaks have energies within 1 eV of the Fermi level, they appear as small shoulders on the large peak near the Fermi level, so their binding energies cannot be determined. No data could be taken below 20 eV because the K Auger $3p$ level conceals the initial-state band features at these photon energies.

A. Occupied bandwidth

The first aspect of the initial-state dispersion to be discussed is the reduction of the occupied bandwidth as compared to the nearly-free-electron prediction. This reduction is due to corrections to the electron's energy from many-body effects.

The photon energy which gives the largest binding energy at $k_{\parallel}=0$ (normal emission) corresponds to a transition from the Γ point. Measuring the binding energy as a function of angle by moving the analyzer off normal for this photon energy produces a dispersion curve of the initial-state energy as a function of $k_{\parallel}$ by using the relation

$$k_{\parallel}=[(2m/\hbar^2)(\hbar\omega+E_i)]^{1/2}\sin\theta\ , \tag{2}$$

where $\hbar\omega$ is the photon energy, E_i is the initial-state energy, and θ is the angle of the detector from the surface normal. Figure 4 shows the binding energy as a function of $k_{\parallel}$ for $\hbar\omega=44$ eV, which produced the maximum binding energy at $k_{\parallel}=0$. The occupied band of the free-electron model has a bandwidth of 2.12 eV and is shown as a dashed line. By performing a least-squares fit of the data to a parabolic band with its minimum at $k_{\parallel}=0$ and with $E_i(k_{\parallel}=k_F)=0$, the occupied bandwidth was determined to be 1.60 ± 0.05 eV. This corresponds to a band with a mean effective mass $\overline{m}=1.33m_e$ as defined by

$$\frac{\hbar^2k_F^2}{2\overline{m}}=E(k=k_F)-E(k=0)\ . \tag{3}$$

The two data points at $k_{\parallel}=-0.455$ and -0.525 Å^{-1} are not included in the fit because they were more than two standard deviations from the curve that resulted when they were included. Negative values of $k_{\parallel}$ correspond to measurements made on the side of the sample normal towards the incident light. The energy at these values of $k_{\parallel}$ is too low because the measured intensity at these negative angles is much lower than at positive angles, due to interference between the two photoemission channels corresponding to the parallel and perpendicular components of the photon's electric field vector.[10] The re-

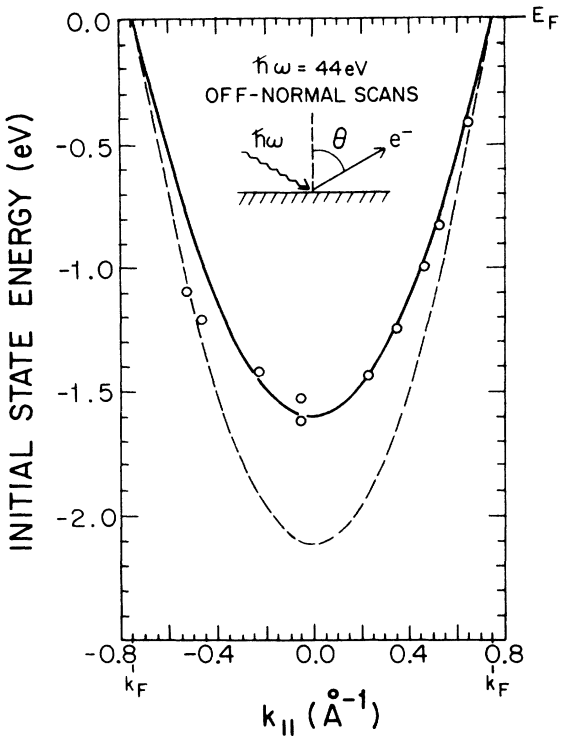

FIG. 4. Initial-state energy as a function of $k_{\parallel}$ for $\hbar\omega=44$ eV. Positive (negative) values of $k_{\parallel}$ correspond to polar angles in the plane of incidence away from (toward) the incident light. Circles are the experimental data, dashed line is the nearly-free-electron prediction, and solid line is the best least-squares fit of the data to a parabolic band. The fit produces an occupied bandwidth of 1.60±0.05 eV. This corresponds to a band with mean mass $\overline{m}=1.33m_e$.

duced intensity makes peak positions more difficult to determine. If these two points are included, however, the fit gives a bandwidth of 1.65 eV.

In the independent-particle picture, the one-electron wave functions and energies are calculated from Schrodinger's equation:

$$(T+V)\Psi_i(\mathbf{r})=E_i\Psi_i(\mathbf{r}) , \tag{4}$$

where T is the kinetic-energy operator and $V=V_{\text{crystal}}=V_{\text{latt}}+V_H$, where V_{latt} is the periodic potential of the lattice ions and V_H is the Hartree potential that describes the time-averaged self-consistent Coulomb potential from all the other electrons. V_H screens the strong ionic potential of V_{latt}, resulting in a weak periodic potential V that can be treated by the NFE model. Because the electrons do not interact in the NFE model (except in terms of the time-averaged Hartree potential), the photoemission excitation spectrum corresponds to one-electron transitions from occupied bands to unoccupied bands.

The next step towards describing real metals beyond the independent-particle approach is to include exchange and correlation interactions between the electrons. This is done by adding to V the term $\Sigma(\mathbf{r})$, which is the static, nonlocal self-energy operator. The inclusion of the self-energy operator will change the ground-state energies from those of the independent-particle model. In addition, excitations can now be screened by the Fermi sea of electrons, so the excitation spectrum measured by photoemission does not correspond to one-electron transitions between bands obtained from the ground-state calculation.

This time-independent model treats the electrons as traveling in the average potential produced by all the other electrons, but this neglects the contribution of the dynamical correlation effects to the electron's energy. Including the time-dependent dynamical contributions makes the self-energy operator energy dependent. This energy-dependent self-energy can be constructed by coupling equations in terms of the noninteracting Green function of the electrons (G), and the screened Coulomb interaction (W). A self-consistent solution of these equations is very difficult because G and W depend on the self-energy. The various theoretical treatments differ in the form of the dielectric function responsible for the screening, the effects contributing to the dielectric function, the form of the electron Green function, and the order in W to which the calculations are carried out. The GW approximation to the self-energy used by Hedin,[11] Northrup *et al.*,[3] and Surh *et al.*[7] truncates the series for Σ to terms of first order in G and W, thereby neglecting vertex corrections. The importance of the higher-order terms in W is still under debate.[12,13]

Hedin used the free-electron Green function and the random-phase-approximation (RPA) dielectric function (i.e., no exchange-correlation effect) to describe the screening.[11] He obtained an occupied bandwidth narrowing of about 10% for both Na and K. For Na, Northrup *et al.* included exchange and correlation in a dielectric function calculated within the local-density approximation (LDA) and used the plasmon-pole model to describe the screening at nonzero frequencies.[3] This resulted in a Na bandwidth narrowing of 18%. By also using the Green function calculated self-consistently from the quasiparticle wave functions and energies, the Na bandwidth reduction was 22%, in good agreement with photoemission measurements.[1,2] Northrup *et al.* concluded that the exchange-correlation effects in the dielectric screening are important for correctly computing the self-energy of alkali metals.[3] The same technique was used by Surh *et al.* for K and produced a narrowing of 25%,[7] in good agreement with our result. Lyo and Plummer showed that it is the local-correction region (i.e., $q=0$) to the dielectric function which is important in the calculation, because holes in the $k=0$ region of the occupied band are screened better by the long-wavelength plasmons than holes at larger k.[2]

Shung and Mahan take a different approach to compute the self-energy.[4] They perform a time-independent calculation within the RPA which neglects exchange-correlation effects. They then calculate photoemission spectra for Na and K by using the photoemission theory of Mahan,[14] which includes the contributions from the surface potential. By including the finite lifetimes of electron states and the interference between surface and bulk contributions, SM calculate a narrowed bandwidth which

agrees with photoemission results from Na and K. Shung and Mahan contend that the RPA-calculated self-energy is correct and that photoemission does not measure the true bandwidth, and that it is these additional effects, neglected in the calculations using the *GW* approximation, that give photoemission the narrowed bandwidth.[4] The contribution of the finite lifetimes of the electron states to the occupied bandwidth should decrease as the photon energy is increased.[4] In the range of photon energies scanned, SM predict changes in the measured bandwidth of ~ 0.17 eV for Na and ~ 0.07 eV for K,[4] yet the photoemission measurements for Na (Refs. 1 and 2) and K (Fig. 3, this work) show no such photon-energy dependence.

Because the real and imaginary parts of the self-energy are connected by a Kramers-Kronig relationship, errors in predicting $\mathrm{Im}\Sigma$ should imply errors in predicting $\mathrm{Re}\Sigma$. $\mathrm{Im}\Sigma$ can be expressed in terms of the lifetime broadening of the bands, which can be measured by photoemission. The full width at half maximum (FWHM) of a photoemission peak at the Γ point is, to first order, due to the hole lifetime and equal to $2[\mathrm{Im}\Sigma(k=0)]$.[15] Hedin[11] and Shung *et al.*[16] produce estimates for $\mathrm{Im}\Sigma(0)$ which are nearly identical and which both underestimate the measured peak width at Γ for Na and K, indicative of errors in their calculations for $\mathrm{Re}\Sigma$. Northrup *et al.*,[3] Surh *et al.*,[7] and Lyo[2] do not calculate $\mathrm{Im}\Sigma$, so a comparison to the data cannot be made.

The calculated occupied bandwidths and lifetimes at the Γ point for Na and K from the many-body calculations discussed are listed in Table I along with the photoemission measurements. The calculations within the LDA using the *GW* approximation and the calculations within the RPA including the surface-potential contributions both agree with the experimental measurements of the occupied bandwidth for Na and K. The RPA calculations underestimate the linewidths at $k=0$, but the existing LDA calculations do not calculate this quantity at all.

Recently, a calculation which includes the vertex corrections neglected by the *GW* approximation was performed by Mahan and Sernelius.[13] They find that the inclusion of the vertex corrections modifies the self-energy to be very similar to that of the RPA calculation for metallic densities. Clearly, the debate of which approximations and computational techniques are more useful is not over.

B. Anomalous peak at the Fermi level

A second deviation of the data from the NFE theory is the sharp peak near the Fermi level for photon energies which should yield no direct transitions. The peak is seen in both photon-energy gaps at about the same binding energy. Deconvolution of the instrumental resolution from the EDC's produces a binding-energy shift for this peak of only ~ 0.02 eV, so the measured binding energy of the peak is not due to instrumental resolution. Looking at Fig. 2, it is difficult to determine uniquely the range of photon energies which produce the anomalous peak near the Fermi level. We have plotted points in Figs. 3 and 7 corresponding to peaks for which the Fermi-level intensity was at least 50% of its maximum value in each photon-energy gap.

Shung and Mahan explained this peak by including the effects on the photoemission signal of the final-state lifetime broadening and the sharp cutoff of initial states at the Fermi level.[4] The final-state broadening is a consequence of the short mean free path of an electron in a final band and is illustrated in Fig. 1 by the grey region around the [110] bands. The inclusion of the short final-state mean free path produces final states in the photon-energy gaps to which electrons initially at the Fermi level can be excited. The sharp cutoff of initial states at the Fermi level accounts for the narrow width of the peak. In the SM calculation, interference between surface and bulk photoemission terms also narrows the observed peak slightly. The SM explanation obviously predicts the intensity of this peak to be reduced in the center of the photon-energy gaps since the electrons are being excited into the tails of the broadened final states. For Na the calculated spectra of SM showed good agreement with photoemission measurements[4,10] of the binding energy and intensity of the peak as a function of photon energy,

TABLE I. Comparison of occupied bandwidths and peak widths ($2[\mathrm{Im}\Sigma(k=0)]$) of Na and K as measured by photoemission to various theoretical estimates which attempt to calculate the contributions of the many-body interactions.

	Na Bandwidth [peak width] (eV)		K Bandwidth [peak width] (eV)	
Theory	Free electron	3.24	Free electron	2.12
	(a)	2.97 [0.91]	(a)	1.89 [0.63]
	(b)	2.44–2.61 [0.94]	(b)	1.46–1.53 [0.64]
	(c)	2.65	(c)	1.65
	(d)	2.53±0.1	(e)	1.58±0.1
Photoemission	(c)	2.65±0.05 [1.2]	This work	1.60±0.05 [0.8]

[a]Hedin (Ref. 11): RPA.
[b]Shung and Mahan (Ref. 4): RPA + surface terms + lifetimes.
[c]Lyo and Plummer (Ref. 2): LDA.
[d]Northrup, Hybertsen, and Louie (Ref. 3): LDA.
[e]Surh, Northrup, and Louie (Ref. 7): LDA.

but the existence of the peak in Na for photon energies outside the photon-energy gap is still unexplained.[4]

A prediction of the peak position in K as a function of photon energy was not given by SM. To see the effects of initial- and final-state broadening on the K band dispersion observed in photoemission, we performed a simple calculation of the peak position versus photon energy obtained using energy and momentum conservation for free-electron bands which included these broadenings. Values for the broadening FWHM were taken from Ref. 16 by taking the FWHM to be equal to 2[ImΣ(K)]: the initial state had a cubic k-dependent FWHM with $\Delta_i(k=0)=0.64$ eV, $\Delta_i(k=k_F)=0$; the final-state FWHM was taken to be a constant, $\Delta_f=5.0$ eV. The density of states was taken to be proportional to the square root of the energy. We used the measured dispersion of the initial state and a constant transition matrix element, but did not include a surface photoemission term. The resulting dispersion is shown as a solid line in Fig. 3. The agreement between the calculation and measurements at point Γ is to be expected because the measured initial state was used in the calculation.

By invoking the final-state broadening, for a given photon energy, there is now a range of states with various reduced momenta k which can satisfy energy and momentum conservation with the occupied initial-state band. The sum of the contributions from this range of final states produces a peak in an EDC with a binding energy which is an average over the allowed range of k. The slope of the initial state, $dE_i(k)/dk$, is largest at the Fermi level, so the range of binding energies for a given range of k is largest near E_F. Also, the sum is weighted towards higher binding energy because of the cutoff of occupied states above E_F. For these two reasons, the final-state broadening has its largest influence near the Fermi level.

At lower energies, the final-state slope $dE_f(k)/dk$ is flatter and the range of allowed k is larger than at higher energies. This has the effect of increasing the binding energy of the resultant peak at lower photon energies. To agree with the measured binding energies in the two photon-energy gaps, a rigorous calculation of the final-state-broadening effect along the lines of that performed in Ref. 4 would have to abandon the assumption that the final-state broadening changes little in the range 20–70 eV. The final-state broadening at ~20 eV would have to be less than that at ~70 eV, which is in contradiction with the calculation of ImΣ done by SM in Ref. 4. The coexistence of the Fermi-level peak with the bulk (110) peak seen for photon energies outside the photon-energy gaps for both Na and K has not yet been explained within the final-state-broadening picture in which these two peaks are one and the same.

The measured intensity at the Fermi level as a function of photon energy is shown in Fig. 5. Shung and Mahan predict [Fig. 5(c)] a reduction of the Fermi-level intensity in the photon-energy gaps. In contrast, the measured Fermi-level intensity is much larger in the lower-photon-energy–gap region [Fig. 5(a)] than for any other photon energies. In the higher-photon-energy gap [Fig. 5(b)] the Fermi-level intensity also goes through a maximum. It

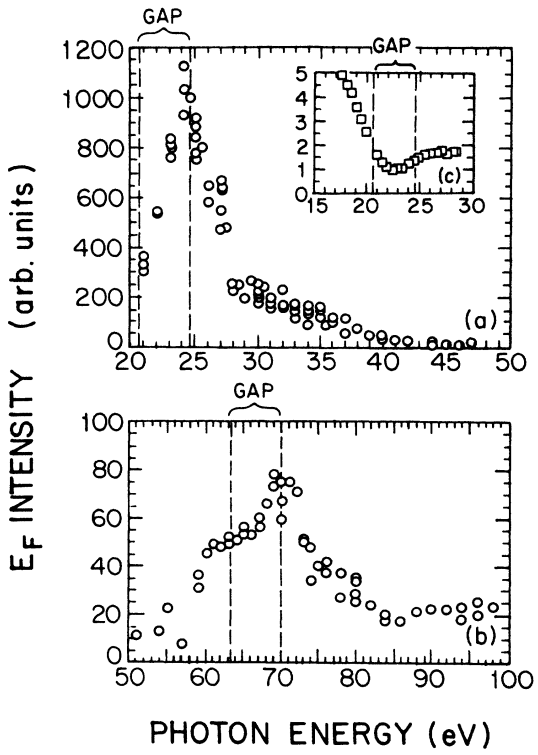

FIG. 5. (a) and (b) are the measured photoemission intensity at the Fermi level as a function of photon energy. (c) is the prediction of SM (Ref. 4). Regions labeled GAP define the photon-energy gaps where no direct transitions are expected in the NFE model.

appears that the final-state-broadening contribution to the intensity is being concealed by the contribution of some additional and unidentified effect.

This additional contribution may be from the surface photoeffect. As detailed by Plummer and Eberhardt,[17] the photoionization differential matrix element can be divided into a number of contributions:

$$\frac{d\sigma}{d\Omega}\sim\left|\frac{2i\,\mathbf{A}}{\omega}\cdot\langle\Psi_f|\nabla V_{\text{bulk}}|\Psi_i\rangle+\frac{2i\,\mathbf{A}}{\omega}\cdot\langle\Psi_f|\nabla V_{\text{surf}}|\Psi_i\rangle+i\hbar\langle\Psi_f|\nabla\cdot\mathbf{A}|\Psi_i\rangle\right|^2, \tag{5}$$

where V_{bulk} is the periodic crystal potential which produces direct interband transitions and V_{surf} is the surface potential. The $\nabla\cdot\mathbf{A}$ term is the contribution to the photoemission signal from the spatially varying photon field $\mathbf{A}$. The sum of the ∇V_{surf} term and the $\nabla\cdot\mathbf{A}$ term is called the surface photoeffect.[17] For an interface between the vacuum and a solid with a frequency-dependent dielectric constant $\epsilon(\omega)\neq 1$, the boundary conditions of Maxwell's equations create a discontinuity in the component of $\mathbf{A}$ normal to the surface. The effect of the $\nabla\cdot\mathbf{A}$ term can be quite large and dramatic, as was shown for the case of Al(100).[18,19]

As measured by Sato *et al.*,[20] the optical conductivity $\sigma(\omega)$ of Na, K, Rb, and Cs are shown in Fig. 6. Looking at the K curve, it is seen that $\sigma(\omega)$, and hence Im$[\epsilon(\omega)]$,

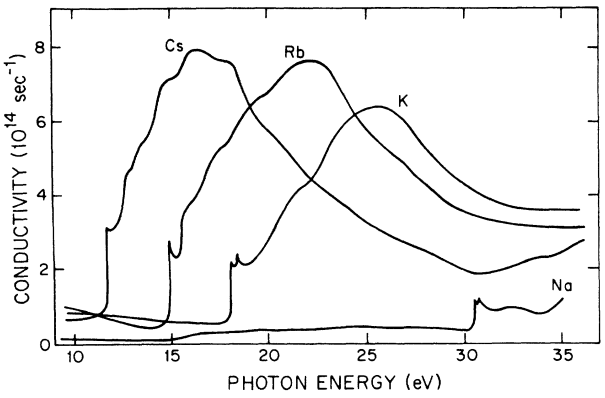

FIG. 6. Optical conductivity of Na, K, Rb, and Cs as measured by Sato *et al.* (Ref. 19) in the photon-energy range 10–35 eV.

peaks in the photon-energy region $20 \leq \hbar\omega \leq 30$ eV, with its maximum at ~26 eV. This energy corresponds to transitions from the $3p$ to the $3d$ levels of K. Using the Kramers-Kronig relationship between $\mathrm{Re}[\epsilon(\omega)]$ and $\mathrm{Im}[\epsilon(\omega)]$, it has been shown[21] that such an absorption peak in $\mathrm{Im}[\epsilon(\omega)]$ corresponds to a rapid variation in $\mathrm{Re}[\epsilon(\omega)]$. The structure in $\epsilon(\omega)$ at these photon energies can make the photoemission contribution of the $\nabla \cdot \mathbf{A}$ term non-negligible. In their calculation of photoemission spectra from K, SM included the ∇V_{bulk} and ∇V_{surf} terms, but assumed a constant photon field, so $\nabla \cdot \mathbf{A} = 0$. A calculation which includes the $\nabla \cdot \mathbf{A}$ term and the interferences associated with it could conceivably account for the large intensity and triangular peak shape[22] at the Fermi level for photon energies $20 \leq \hbar\omega \leq 30$ eV. The previous calculation of the Na photoemission spectra had no need for the $\nabla \cdot \mathbf{A}$ term because, as seen in Fig. 6 and Ref. 23, the optical conductivity of Na in the vuv region is small and changes very little. For Rb and Cs, however, the contribution of $\nabla \cdot \mathbf{A}$ to the photoemission intensity should be larger than in K.

Another proposed explanation of the anomalous peak is the existence of charge-density waves (CDW) in K proposed by Overhauser.[24] Briefly, the exchange and correlation interaction between the electrons in K induces an additional periodicity onto the charge density with characteristic wave vector $\mathbf{Q}$, which is incommensurate with the reciprocal-lattice vectors $\mathbf{G}$. The lattice distorts to neutralize this additional negative charge distribution and small gaps open up in the Fermi surface. Overhauser proposes that this distorted Fermi surface can explain the peaks in the photon-energy gaps.[6] While the CDW mechanism would allow the existence of the peak both inside and slightly outside of the photon-energy gaps, no calculated spectra have been published to compare with measured intensities. At present, the possibility of a CDW mechanism has not yet been ruled out.

It has also been proposed that the anomalous peak is due to a surface resonance centered slightly above the Fermi level having its tail extend below the Fermi level.[5] For the Na(110) surface, Kaiser *et al.*[5] calculated a surface resonance 0.75 eV above the Fermi level. A recent calculation of Rodach *et al.*,[25] however, has concluded that there are no unoccupied surface states in Na(110) lower than 2 eV above the Fermi level. The validity of the surface-resonance explanation of the anomalous peak is therefore in question. To date, no calculations of the electronic structure of the K(110) surface have been performed.

C. Surface umklapp peak

The low-photon-energy region of the initial-state dispersion as a function of photon energy is shown in Fig. 7. It is obvious that the peaks seen for photon energies of 20–33 eV cannot be explained by free-electron bands along the normal direction, [110]. In photoemission, transitions can occur to other final-state bands besides those characterized by a reciprocal-lattice vector normal to the surface as long as both momentum and energy are conserved. The problem is that electrons in these free-electron-like final states are not traveling normal to the surface, so they should not be detected by our analyzer when positioned for normal emission.

The plane-wave final-state picture is justifiable because the short mean free path of the final-state electrons effectively dampens the influence of the periodic cyrstal potential, thereby reducing the band gaps and hybridization between bands. An alternative to using plane-wave final-state bands would be to consider Bloch-wave final-

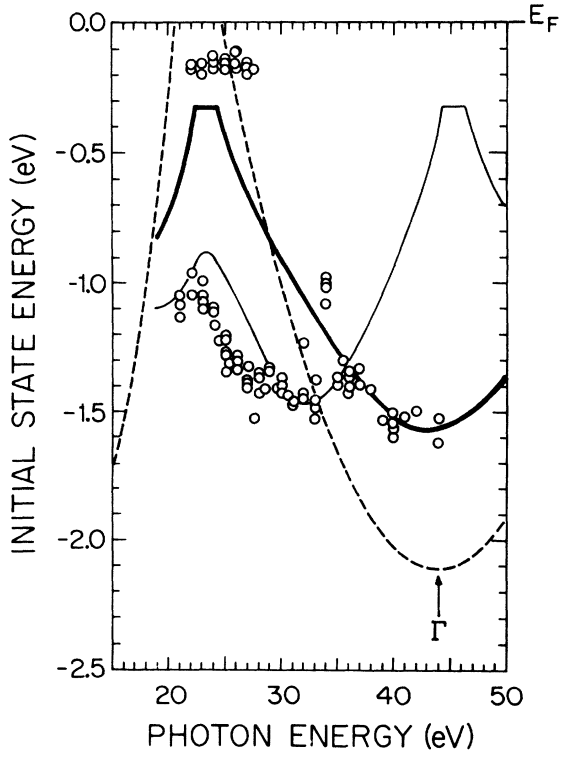

FIG. 7. Initial-state energy as a function of photon energy $\hbar\omega = 15$–50 eV for K(110) normal emission. Circles are experimental data. Dashed line is the NFE (110) dispersion, and the solid lines are our calculations of the NFE dispersions for the (110) and (002) bands including the effects of initial- and final-state broadening and an occupied bandwidth of 1.60 eV.

state bands and sum all the Fourier components in the [110] direction. The equivalence of this treatment to that of the plane-wave final-state bands is clearly explained by Chiang *et al.*[26]

An electron not traveling normal to the surface which traverses the surface has its momentum component parallel to the surface ($\mathbf{k}_{\parallel}$) conserved modulo a surface reciprocal-lattice vector ($\mathbf{G}_{\parallel}$), so it is possible for such an electron to have its $\mathbf{k}_{\parallel}$ component exactly cancelled by a $\mathbf{G}_{\parallel}$ vector, resulting in an electron traveling normal to the surface. Via this surface umklapp scattering, electrons from the Γ points of all the surface Brillouin zones (SBZ) can contribute to the signal from the Γ point of the first SBZ, i.e., at normal emission.

We performed the simple photoemission dispersion calculation described earlier for the bands associated with the (002) rod in **k** space because their initial-state dispersion would reach the Γ point close to the observed photon energy and the very broad peak at 21 eV [as seen in Fig. 2(a)] could be explained by initial and final states with nearly parallel dispersion curves. The resulting curve is shown as the thin solid line in Fig. 7. If the self-energy corrections to the final states were included,[10,16] the calculated dispersion would be shifted towards lower photon energy by $\sim 1-2$ eV, in good agreement with the measured dispersion. This shift is small enough that the fit at higher photon energies is not greatly affected. The bandwidth narrowing due to final-state lifetime broadening is larger for final-state bands with smaller slope $dE_f(k)/dk$.[4] Since the (002) slope is smaller than the (110) slope, the calculated bandwidth from the (002) rod is more narrow than that from the (110) rod. It seems that the calculation of the dispersion along the (002) rod including the broadening accounts reasonably well for the existence of this peak. However, using the surface umklapp mechanism to explain this peak raises some interesting questions.

First, once the case is made for the surface umklapp process, bands along all the rods perpendicular to the surface should contribute to the normal-emission photoemission, not just those along the (002) rod. They can all have their $\mathbf{k}_{\parallel}$ component exactly cancelled by a $\mathbf{G}_{\parallel}$ vector. If they all contributed to normal emission the EDC's would be much more complicated. However, two criteria can be used to eliminate some of the bands along the various **k** rods. Since the surface effects are very important for this mechanism, the peak should be more noticeable in the low-kinetic-energy regime where the mean free path of the photoelectrons in K is approximately one lattice constant.[27] Also, the larger the ratio $|\mathbf{k}_{\parallel}|/|\mathbf{k}_{\perp}|$, the longer a photoelectron will be in the surface region, so the probability of its being scattering by a surface $\mathbf{G}_{\parallel}$ vector is higher. All the final-state bands which satisfy the conditions that the energy of the final state be less than 35 eV (with respect to the Fermi level) and the photoelectron's momentum be more than 45° from the surface normal are shown as solid lines in Fig. 8. Dotted lines show the extension of these bands to higher energies. Photoelectrons in the (002) and $(\bar{1}\,\bar{1}\,2)$ bands travel nearly parallel to the (110) surface, so the probability of being scattering via surface umklapp is greatest for these

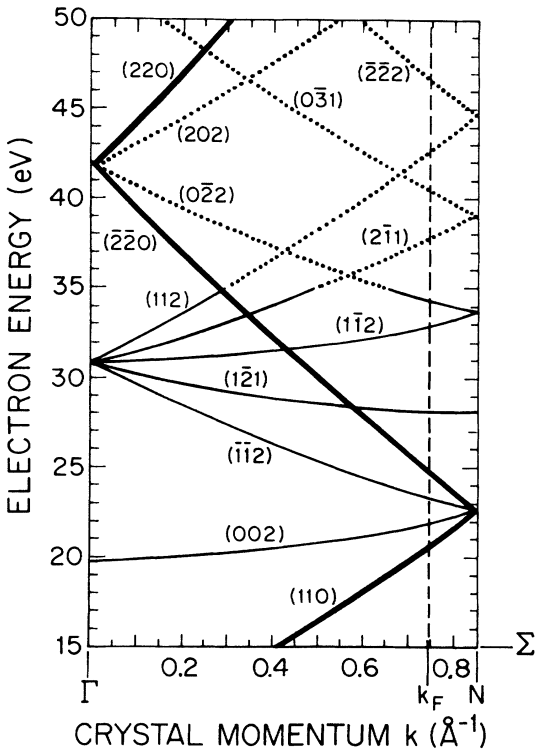

FIG. 8. Dispersion of final-state bands in the Σ reduced zone along various rods in **k** space. The darker solid line signifies the (110) bands. The lighter solid lines signify those bands which pass the criteria of low kinetic energy and large $k_{\parallel}$ momentum component. Dotted lines signify the continuation of these bands to higher kinetic energies.

bands. There is some evidence that the other bands which satisfy these criteria are also seen in normal emission. They could explain the small change in slope of the data seen in Fig. 7 at ~ 28 eV. Note, also, that these other bands should contribute to the intensity at the Fermi level for photon energies where no states were expected. We performed a constant-initial-state (CIS) scan, which is shown in Fig. 9. During a CIS scan both the photon energy and the observed kinetic energy are scanned together to maintain a constant initial-state energy. In Fig. 9 the initial state is the Fermi level. Note the similarity of Fig. 9 to Fig. 5(a). They represent the same function measured in two different ways. Each point in Fig. 5(a) was obtained by setting the photon energy to a particular value, performing an EDC scan, and then measuring the intensity at the Fermi level. In Fig. 9 the Fermi-level intensity was measured as both the photon energy and kinetic energy of the photoelectron were swept together. The CIS scan, minus background, gives the density of final states with reduced momentum equal to the Fermi momentum as a function of photon energy. Because of small variations between the sweep rates of the monochromator and analyzer, the peak positions and intensities in Fig. 9 should only be used as approximate values. The inclusion of the self-energy correction[10,16] to the free-electron final bands seen in Fig. 8 along the (110), (002), $(1\,\bar{2}\,1)$, and $(1\,\bar{1}\,2)$ rods in **k** space gives good agree-

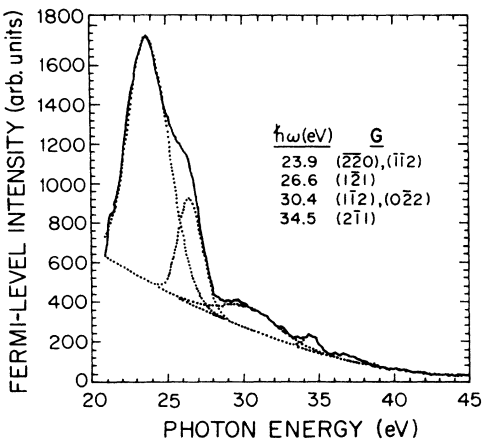

FIG. 9. Constant-initial-state (CIS) scan with $E_i = E_F$ from K(110) normal emission. The background and the four peaks obtained by fitting Gaussian peaks to the CIS scan are shown as dotted lines.

ment to the observed peak positions of the CIS scan.

The second problem with this surface umklapp process is that while it occurs for all ordered surfaces, it is typically an order of magnitude weaker than the standard bulk peak.[26] The (002) peak that we observe, however, is of comparable intensity to the bulk (110) peak. To account for the observed intensity of the surface umklapp scattering, the crystal potential of K at the surface may be larger than previously thought.

Surface distortions may increase the surface potential, thereby producing strong surface umklapp scattering. There are a number of possible distortions the surface could undergo, but only two will be mentioned here. Small amounts of oxygen contamination could distort the K surface, but the surface umklapp peak is seen even on newly deposited films and does not increase in intensity as the sample becomes more contaminated. A more interesting possibility is a planar slip of the first or first few atomic layers of K with respect to the bulk. This would preserve the two-dimensional periodicity seen in LEED, but would change the surface charge amplitude. The low-temperature bulk martensitic phase transition of the alkali metals is thought to be caused by a planar slip of the (110) planes along the $[1\bar{1}0]$ direction.[28] For all of the alkalis, the TA $\Sigma_1[110]$ phonon mode associated with this lattice motion is very soft; for K it is about 2 times softer than for Na and 4 times softer than for Li, as can be seen in Table II.[29] Thus it seems very possible that this slip could occur at the surface where the restoring forces are less than those from the bulk. This mechanism would also be expected to occur in Na, although much weaker than in K. An unexplained weak shoulder on the anonalous peaks observed in the photon energy gap of Na (Ref. 10) could be caused by this surface shear mechanism as seen in K.

TABLE II. Frequencies of the TA $\Sigma_1[\zeta\zeta 0]$ phonon at N ($\zeta = 0.5$) for the alkali metals and some other bcc metals (Ref. 29).

	ν (THz)		ν (THz)		ν (THz)
Li	1.90	K	0.5	V	4.5
Na	0.93	Rb	0.32	Nb	3.93
		Cs	0.2	Ta	2.63

IV. CONCLUSIONS

Angle-resolved photoemission from K(110) has found features similar to those found in Na(110). The measured occupied bandwidth of 1.60±0.05 eV compares well with theoretical estimates, although these estimates differ in the approximations used and the effects to which they attribute the bandwidth narrowing. The source of the anomalous peak near the Fermi level is still unexplained. The measured properties of the anomalous peak in K and the prediction of the final-state broadening picture proposed by SM clearly show discrepancies, but in fairness to SM only their work is detailed enough to make such a comparison. It may be that the behavior they ascribe to the final-state broadening is obscured by a large contribution from an unknown source, possibly a large surface photoeffect. A comparison to calculated spectra and Fermi-level intensities for the CDW and surface-resonance models would be informative. Finally, the observation of a relatively strong surface umklapp peak dramatizes the importance of the surface potential in describing photoemission from K, and may be a clue to surface distortions.

ACKNOWLEDGMENTS

The authors wish to thank E. Jensen and R. Bartynski for their advice during the acquisition of the data, E. Mele and P. Soven for helpful discussions during the writing of this paper, and D. M. Zehner for the use of the Ni(100) crystal. This work was supported by the U.S. National Science Foundation (NSF) under Grant No. DMR-86-10491. The Laboratory for Research on the Structure of Matter at the University of Pennsylvania is funded by NSF Grant No. DMR-88-19885 and the NSLS vuv U-12 beamline at Brookhaven National Laboratory is funded by the NSF Materials Research Laboratories Program through Grant No. DMR-85-19193 and by Oak Ridge National Laboratory through the U.S. Department of Energy.

*Present address: IBM Research Division, Thomas J. Watson Research Center, P.O. Box 218, Yorktown Heights, New York 10598.

[1] E. Jensen and E. W. Plummer, Phys. Rev. Lett. **55**, 1912 (1985).

[2] In-Whan Lyo and E. W. Plummer, Phys. Rev. Lett. **60**, 1558 (1988).

[3] John E. Northrup, Mark S. Hybertsen, and Steven G. Louie, Phys. Rev. Lett. **59**, 819 (1987).

[4]Kenneth W.-K. Shung and G. D. Mahan, Phys. Rev. B **38**, 3856 (1988).
[5]J. H. Kaiser, J. E. Inglesfield, and G. C. Aers, Solid State Commun. **63**, 689 (1987).
[6]A. W. Overhauser, Phys. Rev. Lett. **55**, 1916 (1985).
[7]Michael P. Surh, John E. Northrup, and Steven G. Louie, Phys. Rev. B **38**, 5976 (1988).
[8]C. Allyn, T. Gustafsson, and E. W. Plummer, Rev. Sci. Instrum. **49**, 1197 (1978); B. Tonner, Nucl. Instrum. Methods **172**, 133 (1980).
[9]S. L. Qiu, C. L. Lin, J. Chen, and Myron Strongin, Phys. Rev. B **39**, 6194 (1989); J. Chen, S. L. Qiu, C. L. Lin, and Myron Strongin (unpublished).
[10]In-Whan Lyo, Ph.D. thesis, University of Pennsylvania (1988).
[11]Lars Hedin, Phys. Rev. **139**, A796 (1965).
[12]John E. Northrup, Mark S. Hybersten, and Steven G. Louie, Phys. Rev. B **39**, 8198 (1989).
[13]G. D. Mahan, and B. E. Sernelius, Phys. Rev. Lett. **62**, 2718 (1989).
[14]G. D. Mahan, Phys. Rev. B **2**, 4334 (1970).
[15]E. W. Plummer, Phys. Scr. **T17**, 186 (1987).
[16]Kenneth W.-K. Shung, Bo E. Sernelius, and G. D. Mahan, Phys. Rev. B **36**, 4499 (1987).
[17]E. W. Plummer and W. Eberhardt, Adv. Chem. Phys. **49**, 533 (1982).
[18]Harry J. Levinson and E. W. Plummer, Phys. Rev. B **24**, 628 (1981).
[19]P. J. Feibelman, Phys. Rev. Lett. **34**, 1092 (1975).
[20]Shigeru Sato *et al.*, J. Phys. Soc. Jpn. **47**, 836 (1979).
[21]J. D. Jackson, *Classical Electrodynamics,* 2nd ed. (Wiley, New York, 1975).
[22]K. L. Kliewer, Phys. Rev. B **15**, 3759 (1977); K. L. Kleiwer, in *Photoemission and the Electronic Properties of Surfaces,* edited by B. Feuerbacher, B. Fitton, and R. F. Willis (Wiley, Chichester, 1978), Chap. 3.
[23]H. W. Wolff *et al.*, Z. Phys. **257**, 353 (1972).
[24]A. W. Overhauser, Adv. Phys. **27**, 343 (1978).
[25]T. Rodach, K.-P. Bohnen, and K.-M. Ho, Surf. Sci. **209**, 481 (1989).
[26]T. C. Chiang *et al.*, Phys. Rev. B **21**, 3513 (1980).
[27]David R. Penn, Phys. Rev. B **13**, 5248 (1976).
[28]O. Blaschko and G. Krexner, Phys. Rev. B **30**, 1667 (1984); J. A. Wilson and M. de Podesta, J. Phys. F **16**, L121 (1986); G. Ernst, C. Artner, O. Blaschko, and G. Kraxner, Phys. Rev. B **33**, 6465 (1986).
[29]P. H. Dederichs, H. Schober, and D. J. Sellmyer, in *Landolt-Börnstein: Numerical Data and Functional Relationships in Science and Technology,* edited by K.-H. Hellwege and J. L. Olsen (Springer-Verlag, Berlin, 1981), Vol. 13a.

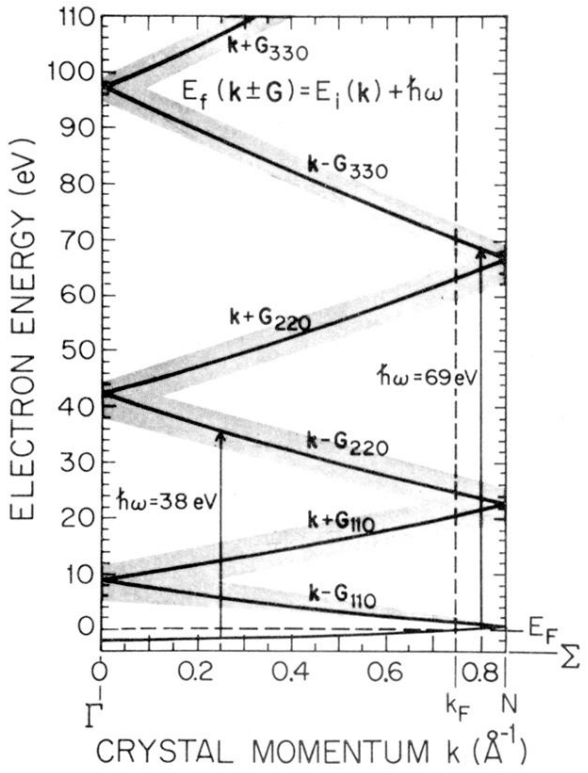

FIG. 1. Free-electron bands along the Σ axis in K. The shaded region illustrates the broadening of the final states due to the photoelectron's finite mean free path. Energy and momentum conservation require photoemission transitions to be vertical in the reduced zone. For $\hbar\omega = 38$ eV the transition should produce a peak about 1.9 eV below the Fermi level in an EDC. In certain photon-energy ranges, e.g., $\hbar\omega = 69$ eV, no occupied states can meet the conservation criteria, so no peak is expected.